Lattice gas modeling of nanowhisker growth

W. Miller
Institute for Crystal Growth (IKZ), Max-Born-Strasse 2, D-12489 Berlin, Germany

S. Succi
Istituto Applicazioni Calcolo CNR, 137 Viale del Policlinico, 00144 Rome, Italy

(Received 23 April 2007; published 5 September 2007)

Building upon the ideas of Gerischer *et al.*, we have developed a cellular automaton for the growth dynamics of nanowhiskers. We present two models for the whisker growth. The first is a simple extension of the surface model, whereas the second includes diffusion on the rim of the whiskers. Results for one-dimensional calculations are presented and discussed, together with a comparison between the two models and with experimental results as well.

DOI: 10.1103/PhysRevE.76.031601 PACS number(s): 81.16.Rf, 02.70.Rr

I. INTRODUCTION

Bridging the huge length and time-scale gap between basic atomistic processes and the formation of mesoscopic structures which form the basis for most material-science applications is one of the major challenges of modern scientific simulation.

Deposition processes of semiconductor films and nanowires growth make two outstanding examples in point. In this paper we will focus on nanowire formation, an emerging topic of high interest for optoelectronic applications. Though nanowires have been successfully grown by different groups (see, e.g., [1–3]) most of the questions on growth kinetics are still under active debate. Two items are of central interest: surface growth processes at the atomistic scale, and second, the evolution of the ensemble of nanowires as a cooperative and self-assembling process. The latter involves areas of some 100 nm—small enough for fluctuations to play an important role.

The kinetic Monte Carlo (KMC) method is one of the most successful simulation techniques for processes on surfaces (adsorption, diffusion, desorption, reactions). Dating back to the papers of Weinberg [4,5] this technique has been applied to many thin film growth systems (see, e.g., [6–10]).

The basic idea behind KMC is the following: instead of tracking the exact dynamics between states i (initial) and f (final), a global transition rate $\mathcal{R}(i\rightarrow f)=\Sigma R_k$ is specified, where R_k is the rate of a specific process k and the sum is running over the ensemble of all possible processes $\mathcal{K}$ on the surface. Only one such process, $k\in\mathcal{K}$, is chosen randomly according to its rate R_k to occur in time step $\Delta t_{i\rightarrow f}$. The latter is given by $\Delta t_{i\rightarrow f}=-\ln n_r/\mathcal{R}$, where $0<n_r<1$ is a random number. KMC is an event-driven simulation—particles are moved one at a time along their own trajectory and according to their own time schedule, while others are sitting idle.

On the contrary, in lattice gas (LG) methods all particles sit on the nodes of a regular lattice, and hop synchronously from one site to another according to a site- and time-dependent probability. The time step Δt_{LG} is fixed and defined by a reference process. The major appeal of LG dynamics, besides natural parallelism, is its mathematical and computational simplicity and efficiency. The down side is that, unless the problem is linear (particle propagating in a passive media) the parallel LG dynamics is not strictly equivalent to the serial KMC dynamics, because all particles move at the same time, so that environmental changes due to forerunners are not taken into account. The LG results are then to be trusted on the assumption that these environmental changes are negligibly small. The latter limitation could be lifted by moving to a mesoscopic (lattice Boltzmann) representation [11,12], whereby environmental changes can be encoded within a local equilibrium reflecting the statistical interactions between particles. However, since this option would neglect all-important statistical fluctuations, we shall not pursue it any further in this work.

Whether KMC or LG is preferable strongly depends on the specific system under investigation. The larger the system, the smaller the time step $\Delta t_{i\rightarrow f}$ in KMC, because of the increasing number of possible processes. If the probability that more than one process happens within this time step, the LG automaton becomes more efficient than the KMC from the computational point of view. In addition, LG automata can be easily parallelized, which facilitates the computation of very large systems.

Let us now consider the typical situation in nanowhisker growth: (i) typical flux is about 1 ML/s (one monolayer per second); (ii) time scale for surface hopping: $\tau=\approx 10^{-8}$ s; (iii) diameters of whiskers are $d_{\text{whisker}}=5$ nm (wanted) to $d_{\text{whisker}}=50$ nm (current stage); (iv) distance between whiskers about $d_{\text{dist}}=5-10\times d_{\text{whisker}}$.

For a reasonable calculation we need about $n_{\text{uc}}=10\times 10$ unit cells ($\equiv$100 whiskers). The number of movements on the surface within one time step can be estimated by $n_{\text{move}}\approx(d_{\text{dist}}\times d_{\text{whisker}})^2 n_{\text{uc}}\tau 0.25 d_{\text{dist}}$. In Fig. 1 n_{move} is plotted against the diameter of the whisker for two different spacings between the whiskers. Except for very small diameters n_{move} is larger than 1, which means that a LG automaton will be more efficient than a KMC.

Another issue is the gap in the time scale between the atomistic processes, such as bond breaking and formation events, which governs the formation of nanoscopic structures (nanowhiskers). On the other hand, the fabrication and growth of such structures requires minutes, if not hours, so that it is clear that a detail time tracking of the atomistic

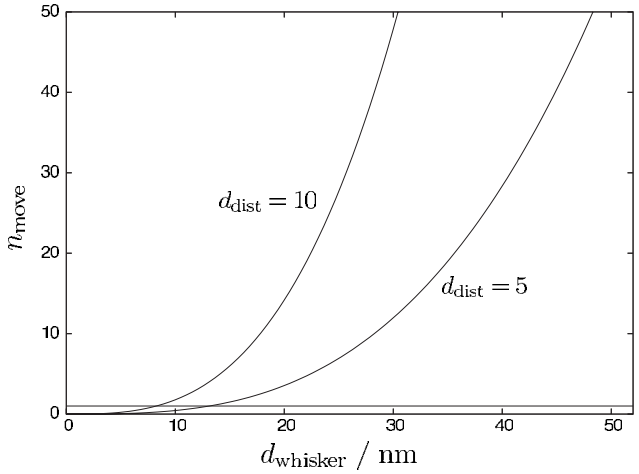

FIG. 1. Estimated average number of movements within a time step as a function of whisker diameter.

dynamics is ruled out on practical grounds. Accelerated (fictitious) dynamics have to be formulated, which retain the essential features of the real ones, without being tied down to atomistic details requiring an unrealistic number of time steps.

II. THE LATTICE GAS MODEL

Here we describe the one-dimensional cellular automaton, which is based on the development of Gerisch *et al.* [13,14]. At each lattice site, labeled by integer i, there is an integer number $h(i)$ of atoms. Adatoms are associated with the uppermost atoms in the stack (see Fig. 2). Overhanging is not allowed. Hence the number of adatoms equals the number of nonempty $[h(i)>0]$ lattice sites.

The adatom dynamics is governed by the number of dangling bonds and the corresponding binding energy. Let $b_{0,\pm}(i,t)$ be the number of free (dangling) bonds of the adatom in its current position i, and the number of dangling bonds it would see by moving one-site left or rightwards, respectively. The dangling bonds lie in the range $1 \leqslant b_k \leqslant 3$ since an adatom is always allowed to grow on top. The basic rule is that an adatom is encouraged to move to positions where the number of dangling bonds is minimized, thereby fostering the evolution towards flat surfaces.

The rate of process $k=0,\pm$ is then given by

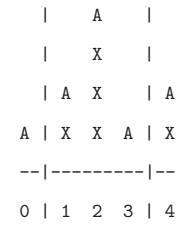

FIG. 2. A periodic (0=3, 4=1) three-site lattice with $h(1)=2$, $h(2)=4$, $h(3)=1$. The adatom $A(1)$ has two dangling bonds (up, left), $A(2)$ has three (left, right, top), and $A(3)$ has only one (top).

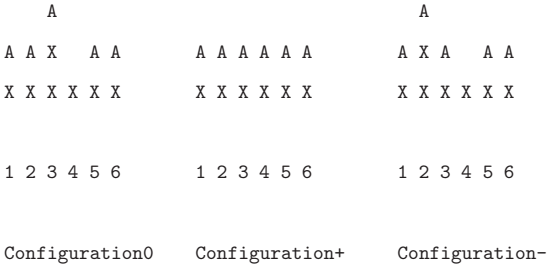

FIG. 3. Configurations associated with the adatom $A(3)$ moving right or left, respectively.

$$R_k = \frac{1}{\tau} e^{-E_b(b_k - b_0)/kT}, \tag{1}$$

where

$$\tau = \frac{h}{kT} e^{E_c/kT} \tag{2}$$

sets the time scale for adatom hopping from one site to another on a flat surface ($b_k=b_0$). In the above, h is the Planck constant, E_c is the corrugation energy, and $k=0$ means "no move," while $k=\pm$ means "move right or left," respectively. The probability of event "k" is then given by

$$p_k = r_k/(1 + r_- + r_+), \tag{3}$$

where we have defined the reduced rates, $r_k=R_k/R_0$.

This formula shows that events such that $b_k>b_0$ suffer a penalty over those with $b_k<b_0$. For instance, transitions which decrease the number of dangling bonds by two units occur on a shorter time scale $\tau_{-2}=\tau Z^{-2}$, while those which increase it take place on a shorter time scale $\tau_{+2}=\tau Z^{+2}$, where we have set $Z \equiv e^{E_b/kT}$. All in all, there are five time scales $\tau Z^{-2}, \tau Z^{-1}, \tau, \tau Z, \tau Z^2$, for the nine possible transitions $b \to b'$, $b, b' = 1,2,3$. Clearly, faster events are more likely to occur and set the pace for the time-marching procedure of KMC simulations. In order to save computer time the values for the five time scales are tabulated once at the beginning.

Based on this rule, a single adatom on a flat surface would experience $b_0=b_-=b_+=3$, so that $p_0=p_-=p_+=1/3$, corresponding to a purely diffusive process with diffusivity $D=\frac{1}{3}$ in lattice units. As a further example, let us consider the "hole filling" process described by the adatom $A(3)$ in Fig. 3 filling the hole at $i=4$. This configuration has $b_0(3)=3$, $b_-(3)=2$, $b_+(3)=1$, hence $p_0(3)=1/(1+Z+Z^2)$, $p_-(3)=Z/(1+Z+Z^2)$, and $p_+(3)=Z^2/(1+Z+Z^2)$. Thus unless $E_b/kT \ll 1$, the hole-filling "move-right" event is selected with near-unit probability $p_+=Z^2/(1+Z+Z^2) \sim 1-1/Z-1/Z^2$.

It is a simple exercise to show that reciprocal "hole-generating" moves suffer the penalty $Z \to 1/Z$, so that "no-move" is the most-likely event.

In the present LG model, all sites are processed in parallel using a global time step dt, while the rates of the various processes contribute to form the fluxes which drive the evolution of the surface profile.

The evolution equation for the number or height of atoms at lattice site $x=idx$ and time t reads as follows:

$$h(i;t+dt) = h(i;t) + [\Phi^+(i-1;t) + \Phi^-(i+1;t) - \Phi^-(i;t) - \Phi^+(i;t)]dt + D(i;t)dt, \quad (4)$$

where $x=idx$ is the spatial position, $t=ndt$ is the synchronous discrete time, and $D(i;t)$ is the local deposition rate. In line with the boolean nature of the lattice gas, at each site $\Phi(i;t)$ are converted to boolean integers $\in\{0,1\}$, according to the following probabilistic rule:

$$0 < \xi < p_0 : \Phi_0 = 1, \quad \Phi_\pm = 0, \quad (5)$$

$$p_0 < \xi < p_0 + p_- : \Phi_- = 1, \quad \Phi_0 = \Phi_+ = 0, \quad (6)$$

$$p_0 + p_- < \xi < 1 : \Phi_+ = 1, \quad \Phi_0 = \Phi_- = 0, \quad (7)$$

where ξ is a random number $\in[0,1]$. Note that the boolean fluxes, jointly with the choice $dt=\tau$, imply that at each time step, the site height $h(i)$ can only change in integer units in the range $\{-2,-1,0,+1,+2\}$, thereby preserving the integer nature of the lattice gas scheme.

The LG dynamics is more efficient than standard kinetic Monte Carlo, because all sites are updated simultaneously in a single time step (intrinsically parallel dynamics). On the other hand, once the system reaches to a configuration such that further moves are inhibited (typically, a whisker on a flat background, see below), the LG dynamics still keeps processing this configuration in vain (zero left- or rightward fluxes) till the next drop falls in. This is a source of inefficiency which must be weighted against the benefits of the intrinsically parallel dynamics.

The lattice Eq. (4) corresponds to a nonlinear diffusion equation in the continuum limit $dx\to 0$, $dt\to 0$, $dx^2/dt \to D_0$, D_0 being the bare diffusion coefficient on a flat surface, $D_0=1$ in lattice units $dx=dt=1$. Leaving the analysis of the continuum limit to a future work, in the sequel we focus on the application of the LG dynamics Eq. (4) to the case of nanowhisker growth.

III. WHISKER GROWTH—MODEL 1

A. LG dynamics

We seed N_w sites $i_1 \cdots i_{N_w}$ with special rules, designed in such a way as to foster whisker growth. The whiskers are distributed on a regular array spaced a distance $d=L/N_w$ lattice units apart, where $L=N_x dx$ is the spatial size of the domain. At each whisker site i_w the outfluxes are set to zero, so that particles can only be absorbed in the first place. Eventually, if the whisker grows too large, particles can be reemitted with probability

$$q_\pm = \frac{1}{2}(1 - e^{-dh^2/2h_{\text{equil}}^2}), \quad q_0 = 1 - q_- - q_+, \quad (8)$$

where $dh=\max\{5h_{\text{equil}}, |h(i_w)-h(i_w\pm 1)|\}$. In the above, h_{equil} sets the typical height contrast beyond which whisker growth is inhibited. More specifically, the growth of whisker gradients in excess of h_{equil}/dx is exponentially suppressed. This spikeness-limiting mechanism can be paralleled to physical desorption process, although a precise mapping in this direction remains to be worked out for the future.

Note that the rule (8) completely overrides the flux rule (5) at whisker sites. This is a desired feature of our model, since whiskers are by definition sites where growth is strongly favored by the underlying chemical-physical processes.

B. Simulation results

The main aim is to assess whether, in spite of the drastic simplification, our LG model is capable of predicting the qualitative features of whisker growth. In particular, we shall explore the way that whisker growth is affected by whisker density and interspacing.

1. Simulation setup

We take $dt=\tau$ and $dx=w$, w being the whisker width. This means that we do not describe any space-time process at the subwhisker scale. In particular, the specifics of the "climbing" dynamics of the atoms along the whisker is entirely hidden within the whisker rules, Eq. (8).

Initial conditions are as follows: $h(i;t=0)=h_0$, plus random fluctuations of amplitude ±1. Periodic boundary conditions at $x=0$ and $x=L$ are imposed.

The deposition process ("rain") is implemented by allowing one drop to fall every n_{rain} steps on a randomly chosen site $1\leqslant i\leqslant N_x$. The quantity n_{rain} is fixed by the deposition rate according to

$$n_{\text{rain}} = \frac{1}{N_x D dt},$$

where D is given in monolayers per second (ML/s), 1 ML corresponding to N_x drops. The main set of parameters is as follows: lattice size $N_x=128$, simulation span $N_t=1000n_{rain}$ (1000 deposited drops/simulation), temperature $T=1000$ K, corrugation energy $E_c=1$ eV, $E_c/kT=11.6$, bond energy $E_b=1.0$ eV (case A), $E_b=0.5$ eV (case B), deposition rate $D=1000$ ML/s, average initial height $h_0=5$, inhibition height $h_{\text{equil}}=10\,000$.

We study the effect of whisker density on the whisker growth process. This is best expressed in terms of the whisker spatial separation

$$d/w = N_x/N_w$$

or, equivalently, in terms of the whisker concentration

$$C = w/d.$$

We change $N_w=\{1,2,4,8,16,32,64\}$ with a fixed $N_x=128$, corresponding to $d/w=\{128,64,32,16,8,4,2\}$. As a general rule, we expect crowding to inihibit single-whisker growth. As an overall figure of merit for whisker growth we take the number of atoms in the whiskers, that is,

$$H_w(t) = \sum_{j=1}^{N_w} h(j;t) \quad (9)$$

or, equivalently, the whiskering ratio, defined as the fraction of drops in whiskers vs total number of drops:

$$W(t) = H_w(t)/H(t). \quad (10)$$

Due to mass conservation, the denominator is known exactly,

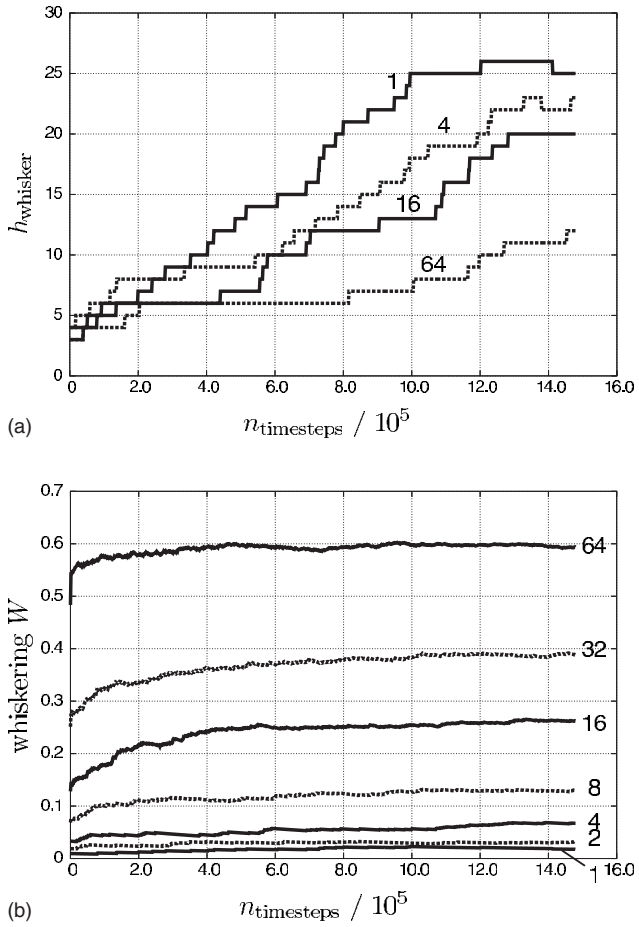

FIG. 4. Whisker height as a function of time (a) and fraction of whisker atoms $W=H_w/H$ (b) for the case with $E_b=1.0$ eV. The numbers at the curves indicate the number of whiskers in the calculation.

$$H(t) \equiv \sum_{i=1}^{N_x} h_i(t) = H(0) + Dt,$$

where $H(0)$ is the total number of drops at $t=0$. In the absence of nonlinear competition, each whisker is expected to develop a mean height $h_{i_w}(t) \sim h_0 + W(t)(Dt/N_w)$.

2. Whisker growth rate: Case A ($E_b=1$ eV)

In Fig. 4(a) we plot the time evolution of the central whisker for the cases $N_w=1,4,16,64$. It is observed that $h(t)-h_0$ lies in the range 5–20 over 1.5×10^6 time steps (corresponding to 1000 droplets deposited at a rate of one each 1500 time steps, a single time step corresponding to about 5 ns.) These values are well below the theoretical limit Dt/N_w, which is 1000, 250, 62.5, 31.5, respectively. This indicates a relatively low whiskering efficiency.

Indeed, the whiskering ratio, as reported in Fig. 4(b), indicates that even with as many as 64 whiskers ($w/d=1/2$, i.e., half filling), only about 60% of droplets fall within whiskers. The remaining 40% remains distributed in the interstitial background. The above data show that the whiskering ratio grows linearly with N_w up to $N_w=16$, indicating no whisker competition in this range. At larger values, i.e., $w/d>1/8$, competition arises and the whiskering efficiency drops down by a factor 2. The data are given in Table I.

TABLE I. Whiskering ratio and efficiency for $E_b=1$ eV and $E_b=0.5$ eV.

	$E_b=1.0$ eV		$E_b=0.5$ eV	
N_w	W	W/N_w	W	W/N_w
1	0.0175	0.0175	0.1828	0.1828
2	0.032	0.016	0.386	0.193
4	0.067	0.0157	0.7672	0.192
8	0.129	0.0161	0.9746	0.122
16	0.263	0.0164	0.998	0.063
32	0.388	0.0121	0.997	0.032
64	0.593	0.0092	0.975	0.016

3. Whisker growth rate: Case B ($E_b=0.5$ eV)

Next we investigate the effects of lowering the dangling bond energy, that is $E_b=0.5$ eV, all other parameters staying the same. In Fig. 5(a), we report the growth of the central whisker for the case $N_w=1,4,8,16,64$. The reduced gap between the time scales, due to the smaller dangling energy ($e^{E_b/kT}$ goes approximately from 9×10^4 to 3×10^2), leads to a less effective spatial redistribution of the spatial profile, hence to a faster growth. In fact, with $N_w \geqslant 4$, the whisker height is seen to overcome the "ballistic" limit Dt/N_w, indicating that, at variance with the case $E_b=1$ eV, the whiskers "eat up" the interstitial background. This is confirmed by visual inspection of the height profiles $h(i)$, as reported in Fig. 6, which clearly shows whiskers standing tall over a nearly zero background.

This indicates that the system is ready to grow faster than permitted by the atom deposition rate D. Indeed, the whiskering ratio $W(t)$ for this case is seen to go top flat ($W=1$), already with $N_w \geqslant 8$, indicating that higher whisker concentrations demand higher deposition rates to grow further. Quantitative data are reported in Table I.

C. Whisker opacity

With a deposition rate of 1000 drops per simulation, setting the parameter $h_{\text{equil}}=10^4$ is tantamount to tagging the whisker sites as literal "black holes," in that the probability of escaping them is virtually zero. It is therefore of interest to estimate the effects of lowering the value of this parameter so as to make the whisker sites "opaque." In Fig. 7 we report the spatial profiles for the case $E_b=0.5$ eV and $h_{\text{equil}}=1000,100$, respectively. From these figures, it is clear that lowering h_{equil} leads to a sizeable reduction of the whisker growth, along with a spreading of the whisker spatial distribution. This is in line with expectations, and it indicates that care has to be taken in the mapping of the microscopic chemico-physical details of whisker growth into an effective coarse-grained parameter such as h_{equil}. As previously commented, in the present work h_{equil} serves as a phenomeno-

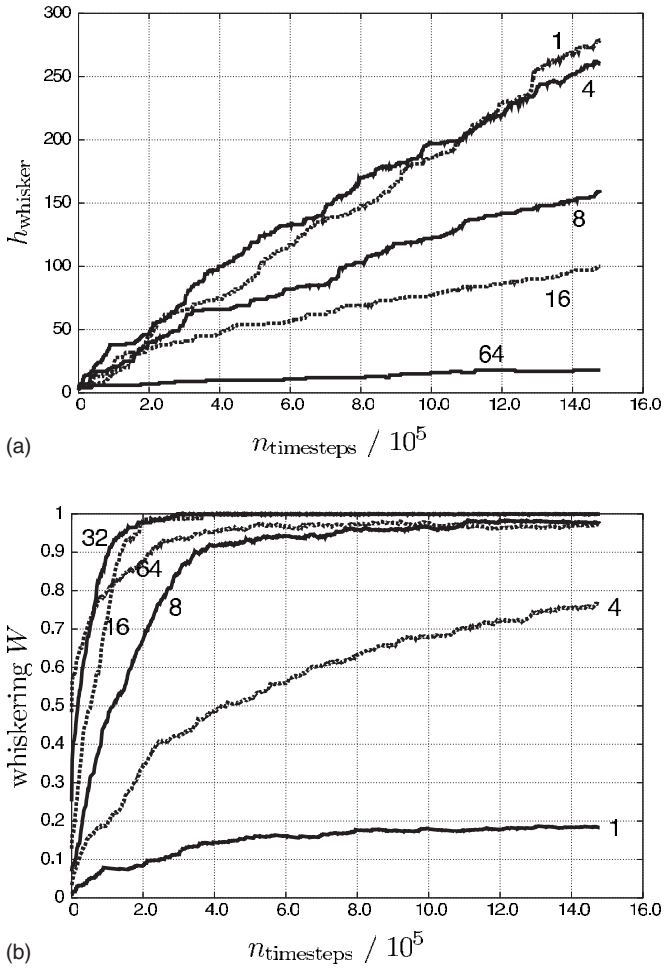

FIG. 5. Whisker height as a function of time (a) and fraction of whisker atoms $W=H_w/H$ (b) for the case with $E_b=1.0$eV. The numbers at the curves indicate the number of whiskers in the calculation.

logical control parameter for the "spikeness" of the height profile. On physical grounds, it could be related to the onset of putative desorption processes, but the details of such mapping remain to be explored for the future.

IV. WHISKER GROWTH—MODEL 2

A. LG dynamics

In this model we treat the diffusion along the rims of the whisker ("climbing dynamics") explicitly with a very simple model. We allow adatoms to diffuse on the rim (climbing up and down), but only in the direction where they do not have another adatom as a neighbor. Possible movements are marked by blue arrows in Fig. 8. Hopping on another adatom (green arrows) is forbidden. This means that the growth of the whisker's diameter is suppressed, as suggested by experimental evidence, according to which whiskers do not grow in diameter but more or less in height only. Lateral growth phenomena, such as those described by the Kardar-Parisi-Zhang paradigm, could easily be described by introducing nonlinear and nonconservative adatom moves, mimicking

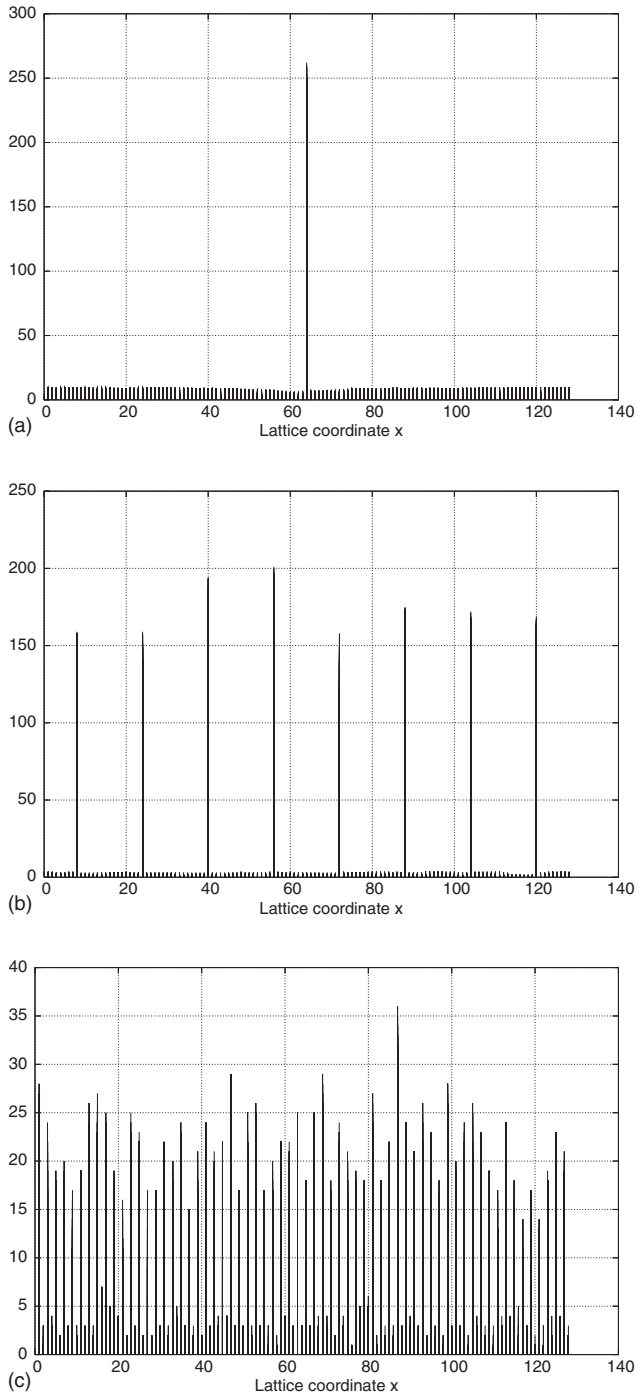

FIG. 6. Spatial distribution $h(i)$ at $t=1.5\times10^6$ for $N_w=1$ (a), $N_w=8$ (b), and $N_w=64$ (c).

the source term $(dh/dx)^2$. Albeit interesting for general interface growth problems, this dynamics is, however, of scanty interest for the case of nanowhisker growth, precisely for the reasons given above.

For the computation of the probabilities we use the same energies (E_c and E_b) as for those on the substrate. Since we use the same corrugation energy E_c for the diffusion on the substrate's surface and the rim of the whisker the time scale is the same. Therefore the probability for staying at the same site is one both for an adatom at the rim and on the substrate.

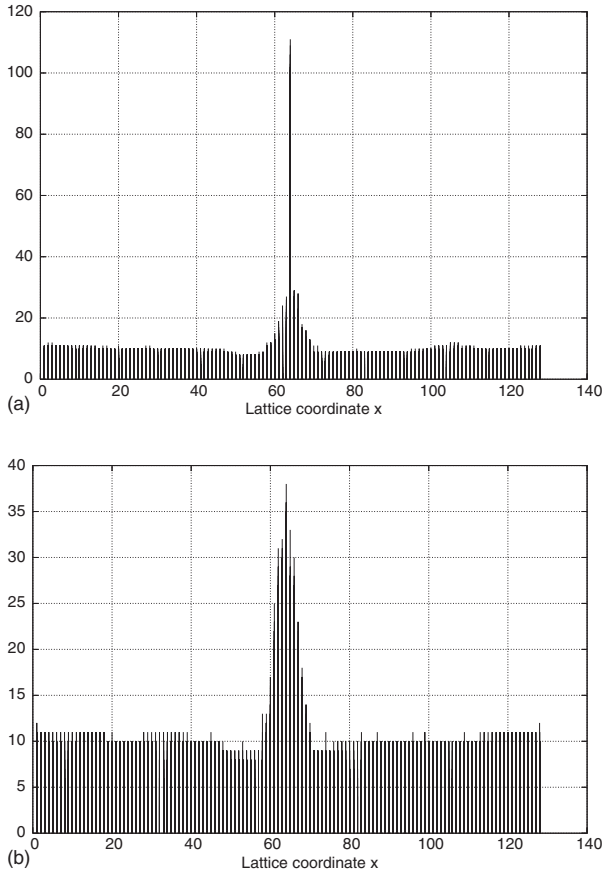

FIG. 7. Spatial profile with $h_{\text{equil}}=1000$ (a) and $h_{\text{equil}}=100$ (b).

If an adatom is sitting at the upmost site of the rim it can enter the droplet with a probability P_{diss}. This probability is an input parameter. We will see that the growth dynamics of the whisker is very sensitive to this parameter. We do not allow any reverse process nor consider any process in the droplet. Therefore once a particle enters the droplet it will be treated as incorporated into the whisker. The whisker height h_{whisker} will increase by $1/(2r_{\text{whisker}})$, where r_{whisker} is the radius of the whisker. Please note that the whisker height is a real number instead of an integer number like $h(i)$. Of course, this is artificial because we do not resolve the surface structure on the top of the whisker; h_{whisker} is the average height of the whisker. The last site on the rim for computations is $\text{int}(h_{\text{whisker}})$.

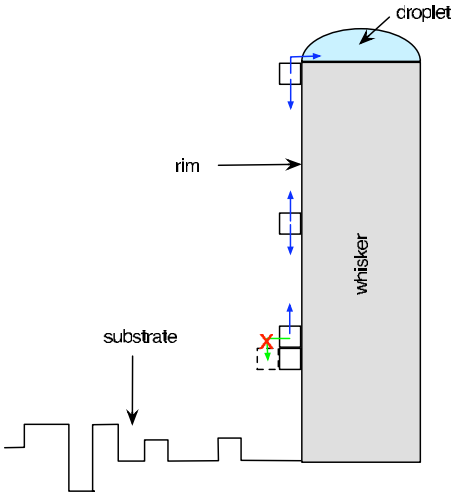

FIG. 8. (Color online) Dynamics on the whisker's rim in model 2. Adatoms on the rim can move freely on the rim but they are not allowed to hop onto another adatom. An adatom at the upmost position on the rim can enter the droplet with a probability P_{diss}.

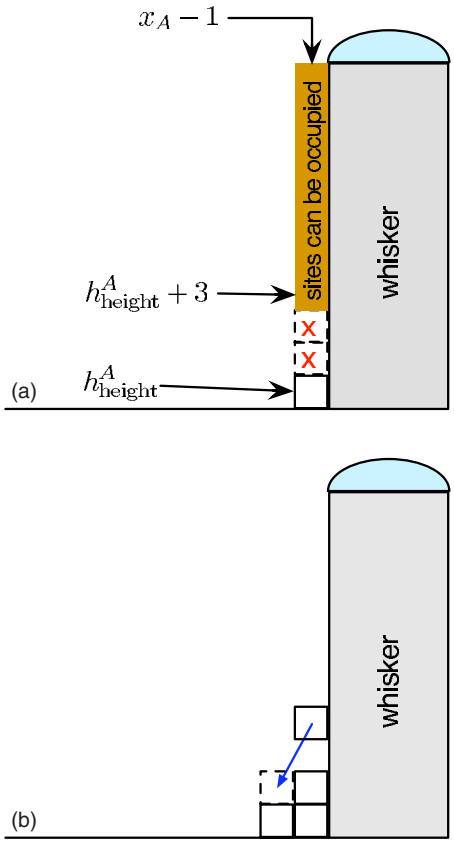

FIG. 9. (Color online) Configuration of sites at the rim of a whisker at its bottom. If the requirement of two empty sites is not fulfilled after the moving step the configuration will be rearranged (b).

In the following we describe the rules to move atoms from substrate to the rim and vice versa. Let the whisker be located at sites x_A to x_B. We consider only the left-hand rim but the same is valid for the right-hand one. Let the height of the substrate at site x_A-1 be h^A_{height}. The atom at x_A-1 with height h^A_{height} belongs to the substrate by definition (see Fig. 9). All adatoms on the left-hand rim have the x coordinate x_A-1. In order to clearly distinguish between adatoms on the rim and the one on the substrate with the same x coordinate (x_A-1) we do not allow adatoms on the rim at heights $h^A_{\text{height}}+1$ and $h^A_{\text{height}}+2$ (see Fig. 9(a)). Therefore the adatom on the substrate at x_A-1, h^A_{height} can move to the position x_A-1, $h^A_{\text{height}}+3$ if this site is unoccupied (see Fig. 10(b)). Then, it becomes an adatom of the rim. Alternatively, it can stay at x_A-1, h^A_{height} or move to left site on the substrate.

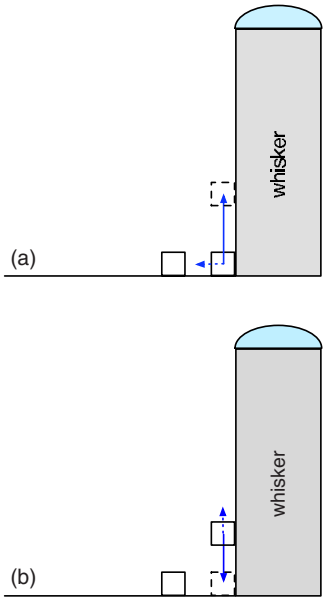

FIG. 10. (Color online) Movements at the edge terrace to whisker. (a) Movement of a particle which is treated to belong to the substrate. It can move to the first possible whisker site.

An adatom on the rim at x_A-1, $h^A_{\text{height}}+3$ can move to x_A-1, h^A_{height} and become an adatom on the substrate (see Fig. 10(b)) through the flux from the gas phase. After the moving step it might happen that there is only one free site between the upmost occupied on the terrace adjacent to a whisker and the first occupied site (see Fig. 9(a) and 9(b)). In this case, the configuration is rearranged as shown in Fig. 9(b).

We do not allow adsorption on the rim or on the substrate at site x_A-1 (and x_B+1).

B. Results

1. Comparison with model 1

First, we will compare the two models for the parameter sets in the previous section. The main difference between the two models is the fact that in model 1 the relative rate of dissolution is defined by E_b. Therefore for $E_b=0.5$ eV not only is the diffusion on the surface significantly enhanced compared to the case $E_b=1.0$ eV but also the hopping onto the whisker. This leads to the very high growth rate of the whisker. Due to numerical reasons the whisker in model 2 has to be at least the width of two units. Therefore we have to rescale the length and time. Let l_1 be, l_2 the lengths of the unit cells in case 1 and 2, respectively. If $l_2=l_{\text{rescale}}l_1$ the time scales are related via $\tau_2=l^2_{\text{rescale}}\tau_2$ in order to keep the diffusion constant the same. Using Eq. (2) the rescaling of the time scale can be translated into a rescaling of the corrugation energy: $(E_c)_2=(E_c)_2+2kT\ln(l)$. Therefore we use now $E_c=0.8808$ instead of $E_c=1.0$. We also have to rescale the particle flux to the surface $(\mathcal{N}_{\text{depos}})_2=(\mathcal{N}_{\text{depos}})_1/l_s$. So we change from 1000 to 2000 ML/s. One can interpret the rescaling as a coarsening of the atomic resolution: one computational unit contains $n\times n$ atoms. We will later show the influence of the coarsening on the dynamics of the system.

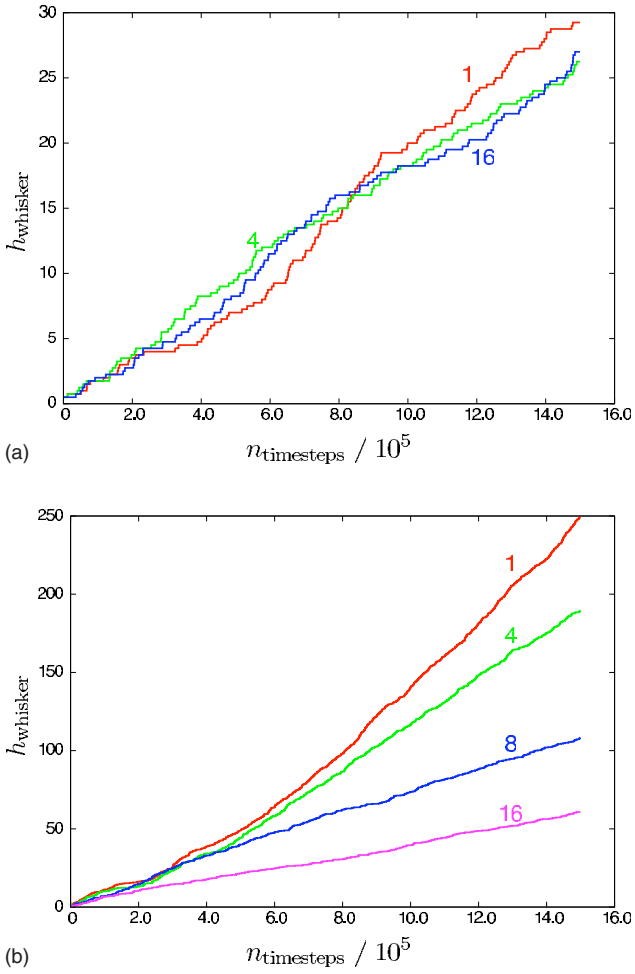

FIG. 11. (Color online) Height of left whisker as a function of time for $E_b=1.0$ (a) and $E_b=0.5$ (b). The numbers at the curves indicate the number of whiskers in the calculation.

We also have to define an adequate probability for the dissolution of a particle into the droplet. In model 1 a particle adjacent to the whisker will have at least one missing dangling bond, i.e., the bond to the whisker. Therefore we define $P_{\text{diss}}=e^{-E_b/kT}$, which results in $P_{\text{diss}}=8.9\times10^{-6}$ and $P_{\text{diss}}=2.99\times10^{-3}$ for $E_b=1.0$ eV and $E_b=0.5$ eV, respectively.

Figure 11 shows the temporal development of the whisker height corresponding to Fig. 4 and Fig. 5. The behavior is similar but for $E_b=0.5$ eV also some differences can be observed. In model 1 the increase of the whisker height is approximately linear in time from the beginning whereas in model 2 there is some time regime of increasing slope before the further growth becomes linear in time. This regime is longer the shorter the distance between the whiskers. Figures 12 and 13 show the surface profile for $E_b=1.0$ eV and $E_b=0.5$ eV. In the latter the rate for dissolution of particles is high enough to provoke a large flux from sides towards the whisker, which leads to trenchlike structure around the whisker. Such structures has been observed in experiments [3] and have been taken as one hint for the assumption that most of the material incorporated in the whisker stems from adsorption on the substrate's surface. When the distance be-

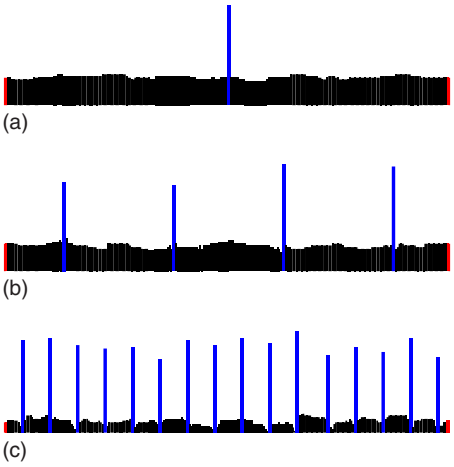

FIG. 12. (Color online) Spatial distribution $h(i)$ for $N_w=1$ (a), $N_w=4$ (b), and $N_w=16$ (c). The run for model 2 ($E_b=1.0$ eV) has been performed with the same parameters as for model 1.

tween the whisker is diminished all material in between is eaten up by the whiskers. Since the total number of sites is small the height of the whiskers is significantly different due to statistical reasons.

2. Parameter studies

a. Variation of resolution. First, we check the behavior of the system when the resolution is reduced. For the atomic resolution, we consider a width of the whisker of 20 and a distance to the next whisker of 2540 atoms. The dynamics has been computed for a total of six coarser systems, as listed in Table II.

We set $E_b=1$ and $P_{\text{diss}}=5\times10^{-4}$. From Fig. 14 it can be seen that in the beginning the growth speed of the whisker is almost the same for all resolutions except for the lowest, where the statistics is too poor. After an initial stage the growth rate is linear until a saturation starts. The start is earlier the higher the resolution. The same effect can be seen more clearly in the whiskering (Fig. 14(b)), where the efficiency is dropping after a certain time for the high resolutions.

b. Different dissolutions. Next we check the influence of the dissolution of the particles into the liquid droplet. The given probability of the dissolution plays an essential role, because once a particle hops into the droplet it can never return and will be treated as instantaneously added to the whisker's top layer. We have performed calculations for various P_{diss} and $T=930$ K, $E_b=0.5$ eV. The deposition rate was still $D=1000$ ML/s, and the corrugation energy $E_c=1$ eV. Figure 15 presents the whisker height for different probabilities. For comparison, the average and maximum heights on substrate's surface are shown. At $P_{\text{diss}}=10^{-5}$, the whisker height is in the range of the maximum height, i.e., no whisker growth can be observed. On the other extreme, for probabilities higher than $P_{\text{diss}}=10^{-3}$, a saturation is reached and the system is diffusion limited.

c. Growth behavior as a function of the whisker's diameter. Schubert *et al.* and Johansson *et al.* analyzed their experiments in order to find a functional relation between the length of the whisker and its radius. The main difference between the experiments is that Schubert *et al.* used molecular beam epitaxy (MBE) [3] while Johansson *et al.* used metal-organic compound vapor deposition (MOCVD) [2]. It is assumed that in the MBE experiments the particles can

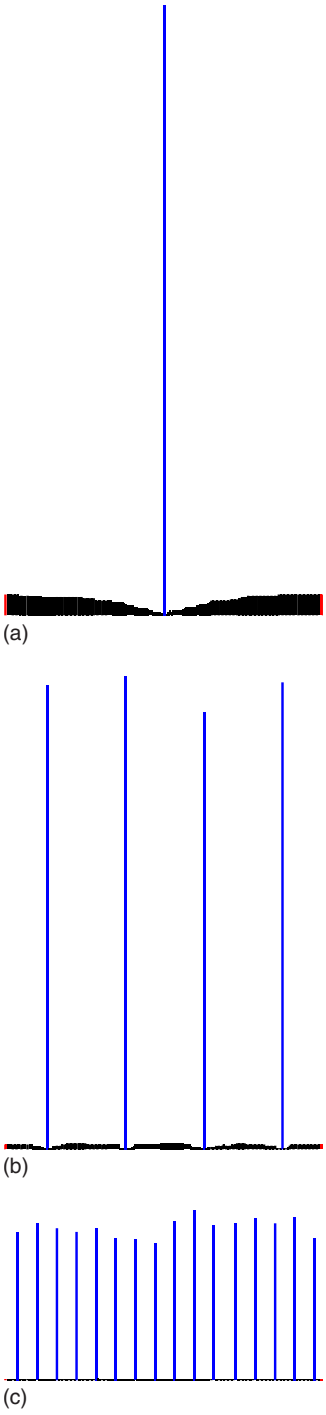

FIG. 13. (Color online) Spatial distribution $h(i)$ for $N_w=1$ (a), $N_w=4$ (b), and $N_w=16$ (c). The run for model 2 ($E_b=0.5$eV) has been performed with the same parameters as for model 1, where the results are shown in Fig. 6.

TABLE II. List of computations with whisker model 2 for comparison with model 1.

N_{grid}	256	512	640	1024	1280	1920	2560
P_{diss}	5×10^{-4}	5×10^{-4}	5×10^{-4}	5×10^{-4}	5×10^{-4}	5×10^{-4}	5×10^{-4}
E_n	1.0 eV	1.0 eV	1.0 eV	1.0 eV	1.0 eV	1.0 eV	1.0 eV
E_c	1.396 eV	1.2768 eV	1.2384	1.1576 eV	1.1192 eV	1.0495 eV	1.0 eV
M_{flux}	100 ML/s	200 ML/s	250 ML/s	400 ML/s	500 ML/s	750 ML/s	1000 ML/s
Iterations	300.000	1.200.000	1.875.000	4.800.000	7.500.000	16.875.000	30.000.000

adsorb on all surface parts, with about the same sticking probability, whereas in the MOCVD the bonds of the metal-organic compound have to be broken before the particular atom can be incorporated. It is also assumed that this procedure is enhanced at the surface of the gold droplets, so that the solving of metallic atoms in the gold droplet is preferred to the adsorption on the terraces or the whisker's rim. In the following, we will only focus on the MBE process, because it is closer to the mechanism described by our cellular automaton model.

Schubert *et al.* described a constant growth rate dh_{whisker}/dt [3]. In our computations, we also observed a linear behavior of the whisker height in time, except in the very beginning. For large times, i.e., large whisker heights, we observe a saturation effect and the growth rate becomes lower. The MBE experiment, which Schubert *et al.* have performed, took place at a substrate temperature of 525 °C and Si flux of 0.05 nm/s. They found

$$h_{\text{whisker}} \propto d_{\text{whisker}}^{m} \tag{11}$$

with $m=-1$ [3]. An exponent $m=-1$ corresponds to the ratio of the contour of the rim to the area of the whisker's top surface. The behavior of the ratio with the diameter of the whisker is the same for one and two dimensions. An exponent $m=-1$ means that the number of atoms in a whisker at a certain time is independent of its diameter. Values in the range $m>-1$ indicate that the number of atoms in the whisker grows with increasing whisker diameter, i.e., the diameter growth demands a mass inflow from the outside, while the opposite is true for $m<-1$.

We have performed several runs by varying both P_{diss}, kT and E_b. From a log-log-plot one can derive a relation $h_{\text{whisker}} \propto d_{\text{whisker}}^{m}$ for all runs (see Fig. 16). But first we observe a significant change in the exponent around a whisker diameter of 50 and for all data the exponent m is smaller than -1. By plotting the number of atoms in a whisker as a function of the diameter we observe a linear increase for all runs

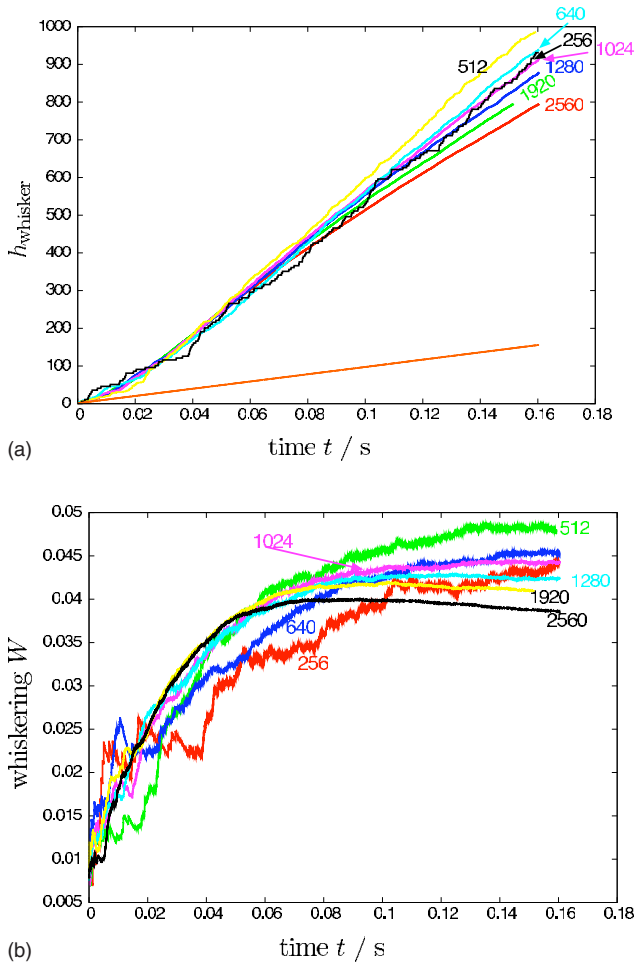

FIG. 14. (Color online) Whisker height vs time (a) and whiskering vs time (b) for different spatial resolutions. The straight line (a) represents the average layer height.

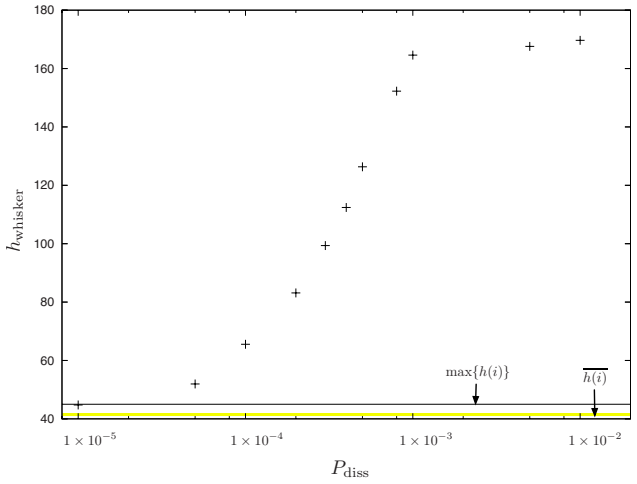

FIG. 15. (Color online) Whisker height at time step 3 000 000 ($\equiv t=4.126\times10^{-2}$ s) as a function of the dissolution probability. The solid line indicates the maximum height on the substrate.

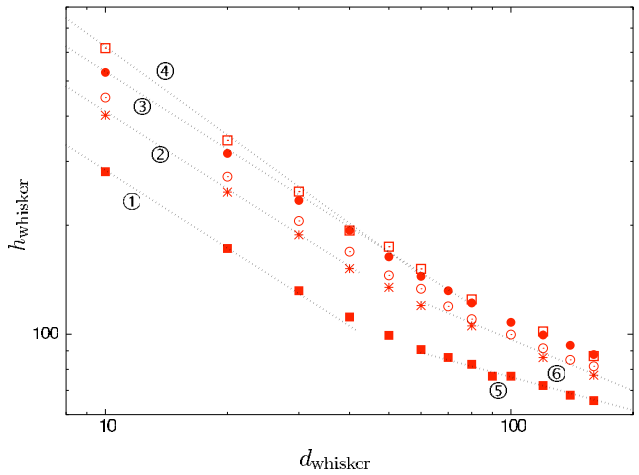

FIG. 16. (Color online) Whisker height as a function of the whisker diameter at time 0.05 s. Filled boxes: $kT=0.086$ eV, $P_{\text{diss}}=2\times10^{-4}$ s^{-1}, $E_b=0.5$; stars: $kT=0.086$ eV, $P_{\text{diss}}=5\times10^{-4}$ s^{-1}, $E_b=1.0$; open circles: $kT=0.086$ eV, $P_{\text{diss}}=5\times10^{-4}$ s^{-1}, $E_b=0.5$; closed circles: $kT=0.086$ eV, $P_{\text{diss}}=1\times10^{-3}$ s^{-1}, $E_b=0.5$; open boxes: $kT=0.100$ eV, $P_{\text{diss}}=5\times10^{-4}$ s^{-1}, $E_b=1.0$. The exponents m are the following: curves 1–3: $m=-0.71$; curve 4: $m=-0.81$; curve 5: $m=-0.30$; curve 6: $m=-0.46$.

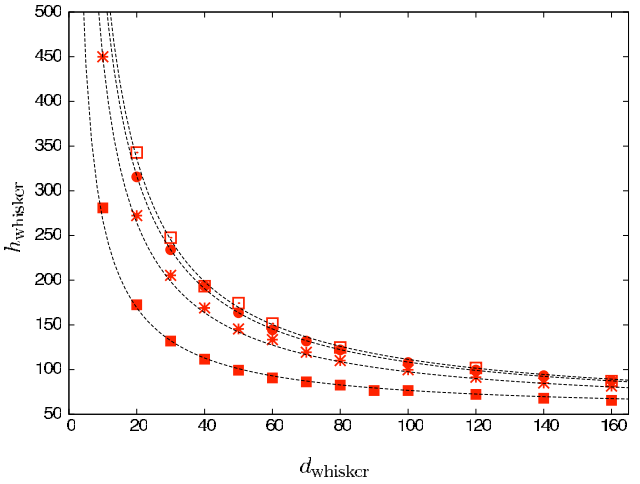

FIG. 17. (Color online) Whisker height as a function of the whisker diameter at $\equiv0.05$ s (iteration=9 349 000 for $kT=0.086$ and iteration=55 366 000 for $kT=0.10$). The dashed lines are according to Eq. (12). Filled boxes: $kT=0.086$ eV, $P_{\text{diss}}=2\times10^{-4}$ s^{-1}, $E_b=0.5$, $\alpha=2500$; stars: $kT=0.086$ eV, $P_{\text{diss}}=5\times10^{-4}$ s^{-1}, $E_b=0.5$, $\alpha=4600$; closed circles: $kT=0.086$ eV, $P_{\text{diss}}=1\times10^{-3}$ s^{-1}, $E_b=0.5$, $\alpha=5700$; open boxes: $kT=0.100$ eV, $P_{\text{diss}}=5\times10^{-4}$ s^{-1}, $E_b=1.0$, $\alpha=6000$.

except for small diameters. In addition, the slope is the same for all runs.

The data for the different runs can be represented by

$$h_{\text{whisker}} = \alpha/(d_{\text{whisker}} + d_0) + \beta \tanh(d_{\text{whisker}}/d_1) \qquad (12)$$

with $d_0=1$, $\beta=52$ for all runs, $d_1=10$ in the case of higher temperature ($kT=0.1$), and in that with the low dissolution probability ($P_{\text{diss}}=2\times10^{-4}$), $d_1=15$ else (see Fig. 17). Unlike the power law Eq. (11), Eq. (12) is not divergent as $d_{\text{whisker}}\to0$, and stays above zero as $d_{\text{whisker}}\to\infty$. Both amendments make full physical sense. In fact, $\alpha/d_0\equiv h_0$ and $\beta\equiv h_\infty$ represent the whisker height in the limit $d\to0$ and $d\to\infty$, respectively. Consequently, the finiteness of h_0 indicates that there would be no atoms in an infinitely thin whisker ("needle" limit), whereas the nonzero value h_∞ means that it would take an infinite number of atoms to fill up an infinitely fat whisker ("pancake" limit).

As already mentioned, after an initial state the growth of the whisker is linear in time, until it starts to deviate due to the long diffusion path on the rim of the whisker. A more detailed analysis for the case with $P_{\text{diss}}=5\times10^{-4}$ and $E_b=0.5$ eV shows that the lines representing the linear growth regime for the different whisker diameters match all at the same time ($t_0=0.005$ s) for $h_{\text{whisker}}=0$. Therefore the height in the linear regime can be expressed as

$$h_{\text{whisker}} = g(d_{\text{whisker}})(t - t_0), \qquad (13)$$

where $g(d_{\text{whisker}})$ is a function of the whisker diameter and t_0 reflects the delay due to the finite time for establishing a steady-state situation of the system. We take the function g from our previous analysis for time $t=0.05$ and get

$$h_{\text{whisker}} = \left[\frac{\alpha_t}{d_{\text{whisker}} + d_0} + \beta_t \tanh\left(\frac{d_{\text{whisker}}}{d_1}\right)\right](t - t_0). \qquad (14)$$

Here we have defined the generalized parameters $\alpha_t=\alpha/t_1$ and $\beta_t=\beta/t_1$, with $t_1=0.045$ s. One can see that for large diameters ($d_{\text{whisker}}\gg\alpha_t/\beta_t$) the whisker height is given by $h_{\text{whisker}}\approx\beta_t(t-t_0)$. On the other hand, in the limit $d_{\text{whisker}}\to0$ the whisker height becomes $h_{\text{whisker}}=\alpha_t/d_0(t-t_0)$. Formally, α_t has the dimension of a diffusion constant, whereas β_t has the dimension of a velocity. Both parameters depend on the incoming flux of particles (see Table III). The higher the flux the shorter is the time to reach a steady-state situation of whisker growth. This means that t_0 decreases with increasing flux (see Table III).

Because we used periodic boundary conditions, in our calculation there will be an influence on the growth if the

TABLE III. Parameters in Eq. (14) for different fluxes of gas particles.

flux (ML/s)	α_t	β_t	t_0 (s)
10	4,200	13	0.265
40	15,600	52	0.165
100	36,500	130	0.13
200	60,000	260	0.075
500	90,000	650	0.02
750	96,000	950	0.01
1000	102,000	1200	0.005
1500	115,000	1600	0.0022

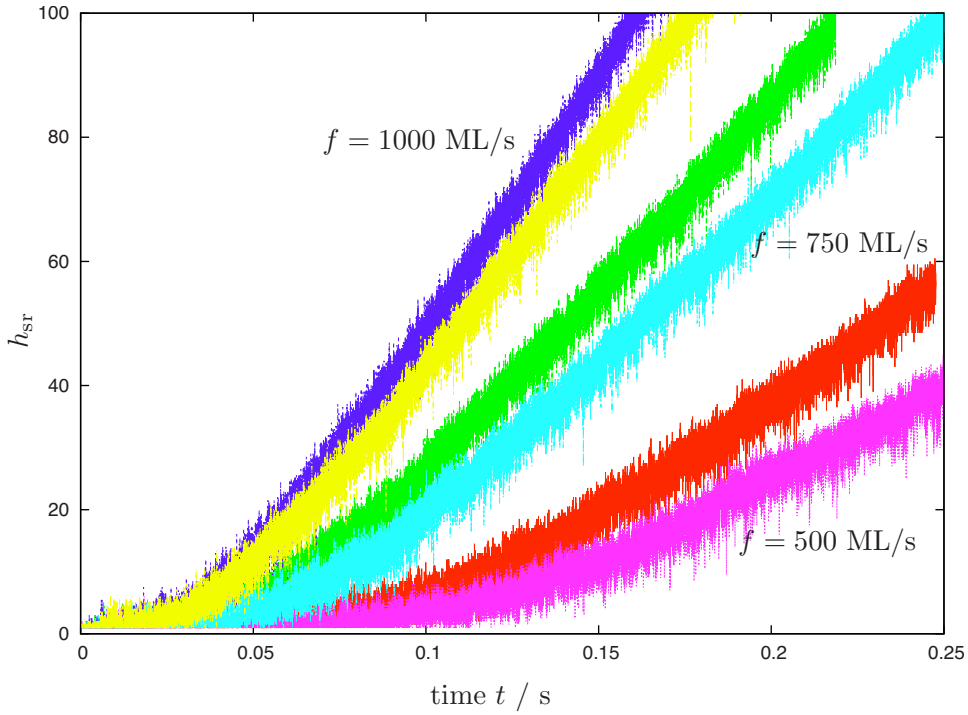

FIG. 18. (Color online) Height of the layer at the rims of the whisker h_{sr} for E_b=0.5 eV and $P_{diss}=5\times10^{-4}$. The upper curve for a particular flux is for $d_{whisker}$=20 and the lower one for $d_{whisker}$=160. The results for three fluxes are shown: 500 ML/s (bottom), 750 ML/s (middle), 1000 ML/s (top). Fluctuations of the height in time are of the same order for all runs.

distance between two whiskers becomes too small. For all computations above, we had one whisker in the computational domain with periodic boundary conditions and a domain width of 2560 grid points. As a result, there was a distance of $2560-d_{whisker}$ grid points between two whiskers. For the case $d_{whisker}$=160, we increased the number of grid points to 25 600. No differences in the growth kinetics were observed.

Next, we present a comparison with approaches of other authors. The growth dynamics of nanowhiskers has been considered in the literature for two different regimes: nucleation-mediated growth [15,16] and diffusion-induced growth [17]. More recently also a combined approach was derived [18]. Because our current model describes the diffusion-induced growth we will discuss our results in the context of the approach of Dubrovskiĭ *et al.* [17]. They derived an equation for the time evolution of the length of the whisker $l_{whisker}$, where $l_{whisker}$ is measured from the epitaxial layer. Note that $h_{whisker}$, which we analyzed so far, is measured from the substrate. Dubrovskiĭ *et al.* considered a homogeneous epitaxial layer without a groovelike structure around the whiskers, which occurred in our simulations and which also have been observed in experiments. We will discuss this question in a moment.

We only consider cases where $R_c/[R(\varepsilon-\gamma)]\gg1$, where R_c is the critical radius at which the direct impingement prevails over diffusion from the surface, $R=d_{whisker}/2$ is the radius of the whisker, γ accounts for desorption from the drop surface and will be zero for all our calculations. Finally, $\varepsilon=(D-V_{surf})/D$ is the relation between the deposition rate D and the growth rate of the surface V_{surf}. The equation for the whisker length by Dubrovskiĭ *et al.* is

$$l_{whisker}=L_d\text{arcsinh}\left(\frac{R_c}{R}+\varepsilon-\gamma\right)\frac{Dt}{L_d}. \tag{15}$$

L_d is the diffusion length at the rim. The analysis of our data was carried in the regime where the growth rate of the whisker was constant, i.e., the change in the whisker height was proportional to time. In this regime, we have

$$l_{whisker}=\left(\frac{R_c}{R}+1-\frac{V_{surf}}{D}\right)Dt. \tag{16}$$

It is difficult to compare our results with this equation, because the question arises of how to measure $l_{whisker}$ in our calculations. We can measure it from the mean average height of the grown layer. Or we can measure it from the height of the layer at the rims of the whisker h_{sr}. This corresponds to the definition of $l_{whisker}$ in the paper [17], because atoms on the rim of the whisker have to overcome this length in order to be incorporated into the liquid droplet at top. Unfortunately, the evolution of h_{sr} is not linear in time in the period where the $h_{whisker}$ increases linearly in t (see Fig. 18). On the contrary, the average layer height is increasing linearly in time and so we use this height as a reference for computing $l_{whisker}$. For $l_{whisker}=h_{whisker}-V_{surf}t$ we obtain from Eq. (14)

$$l_{whisker}=(C-V_{surf})\tilde{t}, \tag{17}$$

where

$$C = \left[\frac{\alpha_t}{d_{\text{whisker}} + d_0} + \beta_t \tanh\left(\frac{d_{\text{whisker}}}{d_1} \right) \right],$$

where $\tilde{t}$ is a shifted time so that $l_{\text{whisker}}=0$ at $\tilde{t}=0$:

$$\tilde{t} = t - \frac{Ct_0}{C - V_{\text{surf}}}. \tag{18}$$

Taking the values for α_t and β_t for $E=0.5$ eV and $P_{\text{diss}}=5 \times 10^{-4}$ (see Table III) both parameters are approximately proportional to D except for very high fluxes,

$$l_{\text{whisker}} = \left[\frac{390}{2R+1} + 1.3 \tanh\left(\frac{2R}{d1} \right) - \frac{V_{\text{surf}}}{D} \right] D\tilde{t}, \tag{19}$$

where we use $R=d_{\text{whisker}}/2$.

Now we can compare Eqs. (16) and (19): From the first term we get approximately $R_c=195$ (in units of lattice sites) and second term in Eq. (19) is of the same order as that in Eq. (16) (it varies between 0 for infinitesimally small R and 1.3 for large R). It is clear that both equations cannot completely match because in the theory of Dubrovskiĭ *et al.* there are no grooves around the whiskers and the system is in a steady-state-like condition from the beginning. In our computations we see that the initialization time can be rather large for small fluxes. Because experiments were analyzed only post-mortem the transient growth behavior could not be observed.

In all computations, the temperature was the same all over the whisker. As long as $h_{\text{whisker}}/d_{\text{whisker}}$ is small this is a good approximation according to the results of the approach of Glas and Harmand [19]. If necessary, a temperature as a function of the whisker height could be easily included into the CA, and we shall leave this as an interesting topic for future research.

V. CONCLUSION

Despite the crude approximations, the present LG model proves capable of reproducing some of the main features observed in experiments. For instance, semiquantitative information on the growth rate as a function of the whisker concentration and the whisker radius can be obtained. Quantitative agreement with experimental situations hinges on a careful fine-tuning of the macroscopic parameters which collect the microscopic chemicophysical details controlling the whisker growth. In this respect, many developments of the current LG model can be anticipated.

ACKNOWLEDGMENTS

S.S. is grateful to the Alexander von Humboldt Foundation for financial support. He also wishes to acknowledge kind hospitality at the Institute for Crystal Growth, Berlin, where this work was performed.

[1] N. D. Zakharov, P. Werner, G. Gerth, L. Schubert, L. Sokolov, and U. Gösele, J. Cryst. Growth **290**, 6 (2006).
[2] J. Johansson, C. P. T. Svensson, T. Mårtensson, L. Samuelson, and W. Seifert, J. Phys. Chem. B **109**, 13567 (2005).
[3] L. Schubert, P. Werner, N. D. Zakharov, G. Gerth, F. M. Kolb, L. Long, and U. Gösele, Appl. Phys. Lett. **84**, 4968 (2004).
[4] K. M. Fichthorn and W. H. Weinberg, J. Chem. Phys. **95**, 1090 (1991).
[5] H. C. Kang and H. Weinberg, J. Chem. Phys. **90**, 2824 (1989).
[6] J. W. Evans, P. A. Thiel, and M. C. Bartelt, Surf. Sci. Rep. **61**, 1 (2006).
[7] D. Choudhary, P. Clancy, R. Shetty, and F. Escobedo, Adv. Funct. Mater. **16**, 1768 (2006).
[8] A. A. Schmid, V. S. Kharlamov, K. L. Safonov, Y. V. Trushin, E. E. Zhurkin, V. Cimalla, O. Ambacher, and J. Petzoldt, Comput. Mater. Sci. **33**, 375 (2005).
[9] C. Cavallotti, A. Barbato, and A. Cavalotti, J. Cryst. Growth **266**, 371 (2004).
[10] G. H. Gilmer, H. Huang, T. D. de la Rubia, J. D. Torre, and F. Baumann, Thin Solid Films **365**, 189 (2000).
[11] W. Miller and S. Succi, J. Stat. Phys. **107**, 173 (2002).
[12] R. Benzi, S. Succi, and M. Vergassola, Phys. Rep. **222**, 145 (1992).
[13] A. Gerisch, A. T. Lawniczak, R. A. Budiman, H. Fukś, and H. E. Ruda, Lect. Notes Comput. Sci. **3305**, 286 (2004).
[14] A. Gerisch, A. T. Lawniczak, R. A. Budiman, H. E. Ruda, and H. Fukś, in *Proceedings of CCECE 2003—CCGEI 2003* (2003), Vol. 2, pp. 1413–1416.
[15] D. Kashchiev, Cryst. Growth Des. **6**, 1154 (2006).
[16] V. G. Dubrovskiĭ, N. V. Sibirev, and G. E. Cirlin, Tech. Phys. Lett. **30**, 682 (2004).
[17] V. G. Dubrovskiĭ, G. E. Cirlin, I. P. Soshnikov, A. A. Tonkikh, N. V. Sibirev, Y. B. Samsonenko, and V. M. Ustinov, Phys. Rev. B **71**, 205325 (2005).
[18] V. G. Dubrovskiĭ and N. V. Sibirev, J. Cryst. Growth **304**, 504 (2007).
[19] F. Glas and J.-C. Harmand, Phys. Rev. B **73**, 155320 (2006).